1. AGENCY USE ONLY (Leave blank) | 2. 21 June 1993 | 3. REPORT TYPE AND DATES COVERED: Scientific No. 4

4. TITLE AND SUBTITLE
Optical Properties of Water Released in Low Earth Orbit

5. FUNDING NUMBERS
PE 62101F
PR 7601 TA 30 WU CP

Contract F19628-91-C-0061

6. AUTHOR(S)
J.A. Gardner, I.L.Kofsky, C.P.Pike*, D.L.A.Rall, R.A.Viereck*, A.T.Stair**, C.A.Trowbridge, E.Murad*, A. Setayesh#

7. PERFORMING ORGANIZATION NAME(S) AND ADDRESS(ES)
PhotoMetrics Inc
4 Arrow Drive
Woburn, MA 01801

8. PERFORMING ORGANIZATION REPORT NUMBER

9. SPONSORING/MONITORING AGENCY NAME(S) AND ADDRESS(ES)
Phillips Laboratory
29 Randolph Road
Hanscom AFB, MA 01731-3010

Contract Manager: Lt Patrick Lofy/WSSI

10. SPONSORING/MONITORING AGENCY REPORT NUMBER
PL-TR-93-2134

11. SUPPLEMENTARY NOTES
*Phillips Laboratory/WSSI, 29 Randolph Road, Hanscom AFB, MA 01731-30
**A.T.Stair Assoc, Bedford, MA 01730; # Radex Inc, Bedford, MA 01730
Reprinted from Proc Soc Photo-Optical Instrumentation Engineers 1754

12a. DISTRIBUTION/AVAILABILITY STATEMENT
Approved for public release; Distribution unlimited

13. ABSTRACT (Maximum 200 words)

Analysis of intensified video photographs of a twilight venting of excess water from space shuttle showed that the ~1 mm diameter stream cavitationally fragments within about 1 m, forming two discrete-particle components and vapor. The images from nearby cameras are dominated by irregular, polydisperse water/ice droplets with sizes comparable with the venting orifice and outward velocity indistinguishable from that of the initially coherent liquid. In contrast the 2¼ km-long quasiconical trail imaged from a distant ground station consists of accompanying submicron ice spherules that were produced by partial recondensation of the overexpanded vacuum-evaporated water gas, which are sublimating at rates that we calculated from the measured falloff of axial sunlight-scatter radiance and the energy balance of progressively roughening ice at 329 km altitude; at low latitudes they cool to 180K in < 1 s, and their radii transition to the Rayleigh-scattering range in ~1 min. The very much larger fragmentation particles come to a slightly higher equilibrium temperature within ~2 min, and persist for a few earth orbits. These three components of the vented water (and other high vapor pressure liquids) radiate and scatter earthshine and solar photons, and the orbital-velocity molecules are also excited by collisions with the residual atmospheric gas, overlaying wide-angle contaminating foregrounds on remote optical sensing from onboard. The particle sizes, densities, and temperatures derived from the visible data are applied in estimating ultraviolet and infrared radiances of the ice/vapor-containing volumes near Shuttle Orbiter.

14. SUBJECT TERMS
Optical properties
Low earth orbit
Vented water
Orbital-velocity molecules
Solar photons

15. NUMBER OF PAGES
12

16. PRICE CODE

17. SECURITY CLASSIFICATION OF REPORT	18. SECURITY CLASSIFICATION OF THIS PAGE	19. SECURITY CLASSIFICATION OF ABSTRACT	20. LIMITATION OF ABSTRACT
Unclassified	Unclassified	Unclassified	SAR

Optical properties of water released in low earth orbit

James A. Gardner II, David L. A. Rall, Christian A. Trowbridge, Irving L. Kofsky
PhotoMetrics, Inc., Woburn, Massachusetts 01801

Rodney A. Viereck, Edmond Murad, Charles P. Pike
USAF Phillips Laboratory, Hanscom AFB, Massachusetts 01731

A. T. Stair, Jr.
A. T. Stair Associates, Bedford, Massachusetts 01730

Alireza Setayesh
Radex, Inc., Bedford, Massachusetts 01730

ABSTRACT

Analysis of intensified video photographs of a twilight venting of excess water from space shuttle showed that the ~1 mm diameter stream cavitationally fragments within about 1 m, forming two discrete-particle components and vapor. The images from nearby cameras are dominated by irregular, polydisperse water/ice droplets with sizes comparable with the venting orifice and outward velocity indistinguishable from that of the initially coherent liquid. In contrast the 2½ km-long quasiconical trail imaged from a distant ground station consists of accompanying submicron ice spherules that were produced by partial recondensation of the overexpanded vacuum-evaporated water gas, which are sublimating at rates that we calculated from the measured falloff of axial sunlight-scatter radiance and the energy balance of progressively roughening ice at 329 km altitude; at low latitudes they cool to 180K in < 1 s, and their radii transition to the Rayleigh-scattering range in ~1 min. The very much larger fragmentation particles come to a slightly higher equilibrium temperature within ~2 min, and persist for a few earth orbits. These three components of the vented water (and other high vapor pressure liquids) radiate and scatter earthshine and solar photons, and the orbital-velocity molecules are also excited by collisions with the residual atmospheric gas, overlaying wide-angle contaminating foregrounds on remote optical sensing from onboard. The particle sizes, densities, and temperatures derived from the visible data are applied in estimating ultraviolet and infrared radiances of the ice/vapor-containing volumes near Shuttle Orbiter.

1. INTRODUCTION

Scattering of visible sunlight from the clouds of droplets formed by liquid water vented from space shuttle *Discovery*[1-4] is a primary source of information about the foregrounds that result from releases of this and other high vapor pressure liquids into the orbital environment. The phenomenology data in intensified video photographs from onboard the spacecraft and the near-nadir Air Force Maui Optical Site (AMOS) provide a basis for quantifying both this optical contamination at other wavelengths and estimating the physical contamination produced by the "flash"-evaporated/sublimed water molecules. Vibrational and rotational emissions from this high-velocity vapor are excited by its collisions with the ambient atmosphere as well as by its thermal and photo-excitation. We calculate here the resulting infrared brightness distributions with the help of a recently developed gas-transport/excitation model[5].

Liquid water rapidly exposed to vacuum has long been known to be unstable against cavitationally bursting[6-10] due to the violent growth of bubbles of vapor ("steam") and dissolved gases within the then-superheated volume. About one-sixth of the injected mass evaporates[11] in cooling the initially 300K stream and its fragmentation droplets to an equilibrium temperature at sunlit orbital altitudes that we have derived as described here. The *Discovery* images also allowed us to bound the fraction of this evolved vapor from a routine operational venting that recondenses as it expands across the gas-solid equilibrium line of the phase diagram of water substance, and to determine the dependence on their distance from Orbiter of the diameters of both these Rayleigh-Mie size droplets and the "geometric"-scattering, polydisperse stream-rupture particles[1-4]. These particles show no evidence of returning to the spacecraft.

Sections 2 and 3 summarize this recent shuttle experiment to provide a background for predictions of the UV-visible-infrared foregrounds and the flow of gaseous water to spacecraft surfaces, which are presented in Sections 5 and 6.

2. EXPERIMENTAL

Largely pure and dissolved gas-free fuel cell product ("supply"[12]) water was forced under pressure directly into *Discovery's* wake on orbit 49 of shuttle mission STS-29 (16 Mar 89), at 19.4 g/s through an electrically-warmed, 0.14-cm opening truncated-conical nozzle. The experiment was planned by the Air Force Geophysics (now Phillips) Laboratory to take place when the flight altitudes were directly illuminated by the sun while the lower atmosphere above the ground station lay in the hard earth's shadow. The spacecraft was moving east-northeast in a 329-km circular orbit as it passed almost directly over AMOS (21°N - 204°E, 3.0 km altitude) about 1 hr before local dawn. Its zenith angle and range, the aspect angle to the retrograde trail (which determines the optical path length through it), and the solar-scatter angle (between vectors from the sun to *Discovery* and from *Discovery* to the groundbased tracking camera) are shown in Fig. 1.

This imaging telescope had an Intensified Silicon Intensifier Target (ISIT) photocathode with S-20R spectral sensitivity (its nominal FWHM photon response, taking into account the small prefiltering by the typically clear atmosphere above the mountaintop observatory, is 0.39-0.65 μm), a 55-cm diameter objective lens providing a 0.5°-diagonal field of view, and electronic gain under operator control. Onboard *Discovery*, SIT zoom cameras of space shuttle's closed-circuit video system viewed from near the tail in its open payload bay and, handheld by a mission specialist, through a crew cabin window about 5 m above and forward of the water-venting orifice (refer to the insert in Fig. 5). These cameras have similar spectral response, and automatic gain control. Figure 2 shows typical images of the cloud of sunlit particles from these close-lying and remotely-located stations.

The AMOS photographs represent a series of view projections and "scene lightings" of a time-stationary physical phenomenon, as both the venting and geophysical conditions remain sensibly constant over the segment of trajectory within the camera's field of regard. Since the optical signal from particles whose dimensions are at least comparable with the light wavelength improves at near-forward scattering angles and from elongated sight paths, we selected for detailed photometric-photogrammetric analysis a video image when *Discovery* was in the northeast quadrant at 60° zenith angle (Fig. 2a). Its high-albedo body is the strongly bloomed feature at the head of the smooth-surfaced, -2½ km-long quasiconical trail. Figure 3 plots the relative radiant intensities per unit distance from the orifice (corrected for aspect angle), i.e., the brightnesses summed along lines perpendicular to the trail's symmetry axis or—in the parlance of rocket exhaust phenomenology—the "station radiance". (This transverse summation removes the effect of the optically-thin particle stream's divergence.) A linear dependence of output current-above-baseline on incident irradiance, which is characteristic of electron multiplier-based image intensifiers operated well below saturation, has been assumed.

The backlit images from the two onboard cameras in contrast showed primarily densely packed discrete particles, which both flickered as they moved coherently outward (indicating tumbling of irregular shapes) and produced variable image irradiances from fixed ranges (evidencing a spread of sizes). Both of these effects have been seen in laboratory tank simulations[10], which indicated that an outer ice "shell" quickly formed on the fragmentation droplets cracks and occasionally even breaks off under the increased pressure from their less-dense, still-unfrozen interior water. This beam of particles, whose dimensions are of the order of the venting nozzle diameter[4,6,8,10], diverges at sensibly the same angle as the trail seen from AMOS (-2/5 radian; see Fig. 2) and projects back to an apex roughly ½ m out from the orifice.

We determined their longitudinal velocities by following several readily-identifiable—and therefore presumably particularly large—water/ice droplets in successive video frames. The 23 m/s velocity with ±35% systematic uncertainty measured is experimentally indistinguishable from the velocity relative to the moving spacecraft of the still-intact (and in fact somewhat contracted[4,6]) liquid stream beyond the conical venting nozzle. The low mean transverse speed obvious from the small angular divergence, along with the narrow spread of the individually-measured longitudinal speeds, shows that breakup of the liquid imparts little momentum to the resulting discrete particles, and indeed the translational energy per unit mass delivered in this fragmentation is extremely small compared with their later changes in heat content.

The transverse-summed radiances in the AMOS frame analyzed are compared in Fig. 3 with predictions of a straightforward model of the submicron droplets' energy balance described in the next Section. The close fit, and also the weak dependence on scatter angle as *Discovery* moves toward the rising sun, shows that this signal at the distant optical station is due to these small ice spherules rather than to the much larger direct products of stream rupture. In the photographs from *Discovery* these unresolved smaller particles appear as a "haze" underlying the bloomed images of the fragmentation particles. Similar heat-balance calculations[1,4] showed that evaporation/sublimation from these very much

larger drops would result in only a $<-15\%$ decrease in their mean cross-sections for scattering visible photons in the ~2-min period during which they traverse the length of trail detectable in the AMOS photographs. In contrast the measured total decrease in radiant intensity per unit length (at distances from *Discovery* beyond where video blooming from its body contaminates the data) can be seen in Fig. 3 to be as much as a factor of 50.

3. INTERPRETATION

As mentioned above, the smaller ice particles are formed by "inverse sublimation" of some fraction of the evolved water vapor. (Rayleigh scattering of sunlight from this gaseous component of the flowfield is far below the radiance thresholds of all the video cameras.) Since the circumference of these recondensation droplets is of the order of twice the wavelength, their cross-sections for scattering visible light per unit mass of water substance are near the maximum physically attainable. Furthermore, their rate of scattering per unit solid angle changes more slowly with direction from the sun than that of the larger ice/water particles (which produce a much stronger forward peak), in agreement with the observed quite small variation of aspect- and downstream distance-normalized station radiance in the sequence of AMOS video images of which Fig. 2a is an example [for scattering at 48°]. The dependence of transverse-summed radiance on distance X from Orbiter is the basis for a calculation of the radius and temperature history of these small droplets. Additionally, the relative irradiances at the onboard image planes from this cloud of unresolved particles and from the distinguishable large particles lead to an estimate of the fraction of the vented-evaporated water that recondenses.

The energy balance of spherical ice (or liquid water not undergoing a phase change) with radius r and uniform temperature T is expressed as [4,8,13-15]

$$(4\pi/3)r^3\rho C\, dT/dt - 4\pi r^2 L dr/dt = \bar{\varepsilon}_e \Omega_e r^2 \sigma T_e^4 + \bar{\varepsilon}_s \Omega_s r^2 \sigma T_s^4 - \bar{\varepsilon}_p 4\pi r^2 \sigma T^4,$$

where the subscripts e, s, and p refer to the thermally radiating earth-and-atmosphere, the sun, and the particle. The terms on the left side are rates of heat loss by cooling and sublimation (or evaporation), and those on the right represent heat gain by absorption of earthshine and sunlight photons and loss by thermal emission. (Heating of the particles by aerodynamic collisions can be readily shown to be negligible at *Discovery's* altitude, and the effect of the additional energy input from sunlight scattered off the atmosphere is very small.) $\bar{\varepsilon}$'s are emissivities/absorptivities of the droplet weighted over the Planck emission spectra of the two assumed-blackbody sources of illumination, and of the gray body itself at T; Ω's are the solid angles subtended by the solar disk and curved earth-and-atmosphere (1.4π ster at 329 km); ρ, C, and L are the density, specific heat, and heat of vaporization of ice (or water); and σ is the Stefan-Boltzmann constant. A second relationship between the two unknowns follows from the sublimation (or evaporation) rate when the probability that departing gas molecules recondense is small, as appears to have been experimentally validated for the coherent column[9]:

$$-dr/dt = 0.27\, P(T)/T^{1/2} = 0.27\, T^{-1/2}\, (2.4 \times 10^{10} \exp - 6110/T),$$

where the numerical value of the multiplier refers to r in cm and vapor pressure P of solid or liquid water in torr. We converted X to time-after-droplet formation t by applying the measured (constant) longitudinal velocity of the distinguishable large droplets, which is justified by the similar angular spreads in the images of the two components of the cloud and the absence of mechanisms that would impart longitudinal momentum to the recombination droplets.

We initially solved these two simultaneous rate equations (numerically) with the assumption that the wavelength-averaged emissivities are proportional to r, a standard result of Mie theory applied to submicron spheres. This dependence ("volume scattering") led to r decreasing at much lower fractional rates than we derived from the AMOS radiances, a discrepancy that is not removed by changing the earthshine temperature--we adopted 280K, representing the average over the nadir hemisphere at low latitudes--, or assigning a different velocity to the recondensation droplets, or assuming polydisperse distributions of their initial radius r_o. The increasing downward curvature of the log-radiances in Fig. 3 is in the direction expected from progressive roughening of the surface of ice exposed to vacuum in the laboratory[13], which has the effect of increasing the imaginary component of its index of refraction and therewith slowing the decrease of its temperature and sublimation rate. An empirical fit to these AMOS data is achieved[3,4] by increasing the $\bar{\varepsilon}$'s by a term proportional to the square root of $(r_o - r)$, a dependence that may arise from the "statistical" nature of the irregular particle erosion (a linear dependence on the decrease in radius gave worse fits to the data). The derived radius and temperature of these small ice particles when they are above threshold in the AMOS images are in Fig. 4.

This dominance of the radiances projected to distant observers by these unresolved small particles and the magnitude and density of the distinguishable irradiance patches from individual large particles in the images from nearby lead to a rough joint constraint on the mean radius of the fragmentation drops and the fraction of vented water that recondenses. Table 1 summarizes the *Discovery* trail parameters estimated from this procedure[4], including an absolute visible brightness. Approximately 2% of the water released, or one-eighth of that which evaporates in the process of freezing and further cooling the remaining mass, forms into droplets whose initial radius r_o is 0.3 μm. Laboratory-tank measurements with ~100 μs-pulsed narrow water streams indicated a roughly similar recondensation fraction with comparable radii of these ice particles[8], which furthermore were within experimental error monodisperse--as we have been assuming.

The constraint showed the mean radius of the fragmentation-product droplets to be 0.13 $\pm$ 0.02 cm, which considering their previously observed[10] irregular ("bowl" and "dish") shapes and broad overall-size distribution should be viewed as an ill-defined average figure. Application of the above energy balance equations led to the results that this radius decreases by $<5\%$ over a 2½ km initial flight path and that these discrete particles survive for several hr[4]. In the first ~1 s diffusion of heat from their interior controls the temperature at their immediate surface, an effect that we took into account both in Fig. 4 and in calculating the rates of water vapor evolution shown in Fig. 5. These radial temperature (and also phase) gradients and--in particular--their shape/size irregularities introduce uncertainty into calculations of the thermal emission from the large drops when they are < ~ 20 m from Orbiter, and their departure from sphericity remains a potential source of error in the infrared radiances after they become isothermal.

4. PHENOMENOLOGY, SCALING

The numerical values presented here refer to relatively pure ~30°C water released near 330 km altitude at low latitudes (or midlatitudes in summer) with the velocity and orifice diameter stated. (The equilibrium particle temperatures have a small dependence on the nadir angle-weighted earth-and-atmosphere radiation model adopted[16].) Since atmospheric drag is negligible over the time scales considered, these results would be independent of the direction in which the stream is released. Larger-diameter, higher-temperature, lower-velocity, more contaminated and gas-laden water columns burst nearer the venting nozzle[6,9], and impurities and lower initial temperatures lead to smaller fragmentation-cone angles (human waste water dumped from shuttle has been observed to form a narrower particle trail than supply water, by a camera held outboard on the spacecraft's Remote Manipulator Arm). Alteration of the equation of state and surface tension of the injected substance by dissolved materials can be expected to lead to quantitative differences in the number and initial size of the two droplet components, and high concentrations of "dye" dopants could increase the absorptivities/emissivities and so change the sublimation rates[7] (although the large water-ice drops are already optically thick across virtually all of the infrared). We note also that low vapor pressure liquids that contain little dissolved gas may not explosively rupture due to boiling, but remain subject to breakup into droplets initiated by fluid stream instabilities[6].

These comments are of necessity qualitative, and in view of the incomplete information about the response of nonreactive liquids to the near-vacuum and radiation field of low earth orbit we have suggested further space and laboratory experiments[7]. The liquid-solid-vapor phenomenology for a given initial temperature, diameter, and flow rate in general depends nonlinearly on the macroscopic parameters vapor pressure, specific heats and heats of fusion and evaporation, thermal conductivity, expansion coefficient, surface tension, and viscosity, as well as on the molecular weight and elastic collision cross-sections of the vaporized material. In consequence scaling of experiment data from one even chemically pure and dissolved gas-free liquid to another is likely to be highly unreliable. Even considering only water, further experience is needed to extrapolate reliably the numerical quantities from this experiment to other venting conditions; the optical sensing-contaminating radiances derived in Section 6 should be viewed in this context.

5. PHYSICAL CONTAMINATION OF ORBITER

The video images from onboard show no evidence of stream-fragmentation droplets drifting backward in the frame of reference of *Discovery* to recontact its body: all move away with sensibly the same speed, that of the radially-relaxed liquid column. (These cameras detected no slower-moving discrete particles, such as have been proposed as originating from fracturing of frost formed on the spacecraft wall near the venting nozzle.) Detailed orbital trajectory calculations[17] have shown that 1-mm ice particles would not collide with Shuttle Orbiter on its subsequent passes, at all angles relative to its flight path that the liquid stream may be injected. Since the much shorter-lived recondensation droplets have the same outward velocity, they also do not return to physically contaminate the spacecraft.

As mentioned, the intensified-video photographs do not detect the unrecondensed water, nor does scattering of sunlight from the droplets provide information—other than an estimated stream-breakup distance—about the rates at which this gas is evolved. (The "flash" vaporization that follows from the exponential dependence of equilibrium vapor pressure on surface temperature is a far more important source of contamination than the indirectly-observable much slower sublimation from recondensation particles, as will become apparent shortly.) Since the vapor comes off with much greater thermal speeds in the spacecraft's reference frame than the directed outward velocity of the stream (of order 600 m/s[9], and to a good approximation isotropic) some fraction of it recontacts exposed vehicle surfaces. Furthermore, these return fluxes are increased and their angular distributions broadened by scattering of water gas from the atmosphere[5,18,19].

An estimate of the vapor production rates from current theory[6] and laboratory vacuum tank measurements[9] on ~1 mm diameter, 300K water streams appears in Fig. 5. The calculation considers only conductive rather than convective internal heat transport (except as the somewhat supercooled liquid explodes at X = ½ m, where the resulting droplets are taken as becoming isothermal at its radially-averaged temperature) and also neglects heating by redeposition of vapor, which appears to be justified by the experiment data. Despite the approximations in the existing theory for cylindrical[6] or spherical liquid geometry, and the uncertainty in the (assumed uniform) water temperature upon injection and breakup distance, the predicted gas-evolution rate summed along X is satisfactorily close to the aforementioned thermodynamic value of one-sixth. We are currently developing a Navier-Stokes equations-based numerical model[7] of the coupling between the two phases that will provide an improved spatial distribution of the vapor escape rates.

This vaporization/sublimation profile, with the further (good) approximation of isotropic free-molecular flow and consideration of the finite diameter of the diverging gas source, allows straightforward calculation of the direct fluxes to exposed surfaces of Orbiter and its instrumentation. For example onto its port-side wall 1 m from the orifice these fluxes are of order 10^{17} molecules/cm^{2}s, or 10^{-2} monolayers in each second of routine water venting. With its payload bay doors closed the spacecraft's body intercepts roughly half of all the vapor initially directed into its starboard hemisphere, producing an extended gas penumbra; and (as the elevation diagram in Fig. 5 shows) the open port-side door shields instrumentation inside the bay from direct exposure to the close-in stream region where most of the gas molecules originate. The evolution rates also serve as input to theoretical calculations[5,19,20] of the contamination by molecules backscattered from the ambient atmosphere and one another (and at least in principle, from control rocket exhaust and outgas species), and—in particular—of the resulting infrared radiance distributions. Direct simulation Monte Carlo calculations of the concentrations of and impact-excited radiances from water molecules exhausted from space shuttle's control engines (at ~½ its orbital speed) indicate that the molecule densities in its bay are strongly dependent on the angle between outflow axis and trajectory even at 600 km altitude[5]; another rarefied gas dynamics model[19] shows substantial buildup of density off ram surfaces at the spacecraft's lowest operating altitudes. A planned extension of Phillips Laboratory's "SOCRATES"[5] Monte Carlo approach to apply innermost computational-mesh spacings comparable with the dimensions of Orbiter will provide quantitative information about the flow of reflected water molecules to its payloads.

6. UV AND IR FOREGROUNDS

Table 2 is a brief qualitative overview of the optical radiations from the three components of the water trail at wavelengths outside the visible range of these *Discovery* video data. The thermal emissions and scattering of earthshine and solar photons from the particles are localized in the image regions shown in Fig. 2, while the collisionally-excited infrared emissions from the vapor originate from all directions around the spacecraft (as is illustrated in Fig. 7).

6.1. Particle stream

Calculation of brightness distributions from the array of discrete liquid/solid particles in effect reduces to exercises in applying standard electromagnetic wave-interaction and -generation theory to dielectric droplets with the radii, temperatures, and spatial densities derived above. The primary sources of error in the computed foregrounds would be the departure from sphericity of both types of particle and uncertainties in the optical constants of ice at their low temperatures[16,21]. Since the diverging trail is optically thin at all wavelengths (as can be readily shown), its radiances in general vary with (X sin [aspect angle])$^{-1}$, the product of sight path length through and mean density within it. Scans transverse to the longitudinal direction in the AMOS video images[4] indicated that the approximation of constant particle concentration at each downstream distance X within the 2/5-radian fragmentation quasicone should be applied in estimating infrared and ultraviolet brightnesses in sensor projections that intercept the trail away from its long axis.

In the ultraviolet, intensities of radiation from the fragmentation particles (which are "geometric" scatterers) fall off with decreasing wavelength due to the decrease in spectral irradiance of sunlight. In contrast radiation from the recondensation particles would show a complex dependence on wavelength and X--that is to say, r--for size parameters $(2\pi r)/(\text{wavelength}) > \sim 2$, where Rayleigh and "Mie" scattering give way to essentially geometric cross-sections. Indeed, at some wavelength/X ratios and photon scattering angles the UV brightnesses of the trail can exceed its measured mean over the visible range (see Table 1). A sunlit water venting has recently been photographed in the vacuum ultraviolet, from the bay of space shuttle on mission STS-39[22]; the images appear similar to Fig's. 2b and 2c, as would be expected for r_o = 0.3 μm near the spacecraft.

In the infrared, the ~mm particles are optically thick while these ≤ 0.3 μm ice particles are inefficient scatterers-radiators except near 2.7 μm[16]. The large-droplet component thus dominates the radiances even in projections to distant sensors, suppressing the severe spectral structure characteristic of the small droplets. That is, through virtually all of the IR thermal emission from the fragmentation particles exceeds solar and earthshine photon scattering by the recondensation particles, the opposite of the situation in the visible. Table 2 presents estimates of the radiances viewing normal to the trail centerline at large and small X in long- and short-wavelength infrared bands applicable in surveillance, made from the Planck radiation from the fractional area covered by the dilute array of blackbody spheres at the temperatures derived in Fig. 4 with a correction in the 3-5 μm interval for scattering of sunlight (which despite the very low droplet reflectivities would be comparable with their thermal emission at low T). In view of the uncertainties from the actual particle shapes, sizes, and densities within sight paths, and the potential error from assuming isothermality at $X < \sim -20$ m (where the large droplets may be optically thin at some wavelengths over outer radial shells with significant temperature gradients), we have stated only the order of magnitude of these spectrally-continuous infrared brightnesses "looking in" perpendicular to the quasiconical particulate trail. Looking out from Orbiter into the relatively small solid angle that it occupies, the foregrounds would obviously be greater--very much so in some projections--because of the smaller view aspect angles.

As the temperatures of the droplets become less than the effective radiating temperature of the earth-and-atmosphere, the vented water volume--like most meteorological clouds--would exhibit "negative [infrared] contrast" in nadir-directed views. This effect is small since the emissivities in columns normal to its long axis are only 10^{-6} - 10^{-3} between X = 1 km and 1 m. Nonetheless even at 2 km from the venting orifice the radiances at the IR "window" wavelengths considered in Table 2 exceed those from the atmosphere's limb at orbital tangent altitudes[23] by at least an order of magnitude. At ~10 m intercept distances of fields of onboard sensors, these foregrounds from the more concentrated particles cloud would interfere with Shuttle Orbiter-based radiometry of the limb at tangent altitudes as low as 30-40 km.

6.2. Water vapor

The major fraction of the gas evolved expands near-isotropically into the atmosphere from a source whose dimensions are comparable with those of Shuttle Orbiter (the aforementioned back-side penumbra being partly filled in by scattering). A straightforward calculation shows that the column densities of water molecules become high enough to perturb the ambient airflow only within a few m of the venting orifice, which is much less than the size of the spatial cells typically used in numerically computing[5,18] volume rates of scattering and radiation near spacecraft. In consequence the body of thought on excitation of outgassed water[18,19,24-28], considered to come off after ~1 day in orbit at roughly one-hundredth the rate at which molecules evaporate/sublime from operational water dumps (as well as on the flowfield of the more energetic rocket-exhaust species[5]), can be brought to bear in predicting the contaminating scene brightnesses. As infrared radiations from this outgas have already been found to interfere with space shuttle-based astrophysical spectroradiometry[24,26], IR foregrounds from the gas evolved from vented water should be readily observable.

These emissions arise primarily from impact excitation of rotational and low-lying vibrational states of neutral and ionized (by charge exchange) H_2O molecules, and formation of OH (hydroxyl) radicals. Resonant and fluorescent scattering of earthshine and sunlight by the vapor, and its thermal excitation[25,28] as it leaves the about-260K condensed stream (Fig. 5), are further sources of optical foreground; see Fig. 6. At the 2½ - 3½ eV center-of-mass translational energies available in collisions with ambient air single-mode, multimode (for example 011 and 110), and multiquantum (020) vibrational levels of H_2O are accessible[26]--these are also populated by the radiation field--, and the fourth vibrational state of OH can be reached in excitative reactions of H_2O with the atmosphere's relatively abundant oxygen atoms. Thus combination-band and overtone photons as well as the familiar single-quantum radiations are expected, principally from within an elastic-collision mean free path from the spacecraft. The IR spectrum includes, in rough order of intensity

– the commonly-encountered strong stretch- and bending-mode fundamental sequences of H_2O near 2.7 and 6.3 μm, rotationally broadened (to an extent that is not known, and would be best determined by on-orbit spectroscopy of evolved water vapor);
– the fundamental vibrational cascade of OH extending above 2.8 μm, also similarly broadened (and whose excitation cross-sections at orbital impact velocity also lend themselves to measurement in space experiments);
–spectrally widespread rotational lines of neutral and singly-ionized water molecules, in which about equal radiances are expected in the 5-16, 17-22, and 23-28 μm wavelength regions[18];
– stretch- and bending-mode fundamental bands of H_2O^+ near 3 and 7 μm, from the high cross-section[29,30] charge-exchange reactions with ionospheric O^+;
–the OH first-overtone sequence centered at 1.6 μm (the second and third overtone are much weaker);
– intercombination and mode-transfer bands from the two water species, primarily near 1.9, 3.1, and 4.7 μm.

(The electronic bands in the ultraviolet and visible, and as mentioned Rayleigh scattering, are extremely weak.)

Each water molecule is photo-excited about once per 1000 s in the 6.3 μm transition (010–000, mostly by earthshine) and once per 4000 s in the 2.7 μm stretch modes[27] (001 and 100–000, by sunlight). In addition $1\frac{1}{2} \times 10^{-4}$ of the molecules evolve from the liquid stream and fragmentation droplets in the 1/20 s-lifetime 010 state, from which they radiate over a ~30 m (exponential) path: and a much larger fraction comes off in much longer-lived rotational states, from which arise comparable total "look-out" radiances[28] in long-wavelength infrared photons. At the air densities where space shuttle normally operates excitation by collisions as noted proceeds more rapidly, resulting in predicted radiance distributions (in "look-in" projections, to emphasize the radial and angular dependences of the contaminating emissions) such as are illustrated in Fig's. 6 and 7. These were calculated by the aforementioned direct-simulation Monte Carlo method[5]. We adopted the cross-sections for elastic scattering and impact excitations previously applied[5,18], and neglected both cascade population of upper vibrational states of H_2O (which are thought to increase its emission rates by ~60%[26]) and rotational lines from H_2O^+ (a smaller additional effect). In view of the well-known large uncertainty in the cross-sections for excitation–and even for elastic processes–, omission of thermal and photo-excitation, and the approximation of an isotropic vapor source (both shielding of the flow by Orbiter's body and the low-level continuing input of molecules sublimated from both size particles at X's beyond the innermost cell of the computational grid are inadequately considered), these predictions of the infrared brightnesses should be considered as less than fully reliable.

Figure 6 is a simple scaling-up to the unrecondensed vapor evolution rate (further reduced by one-quarter as a first-order simulation of the "loss" due to Orbiter's body) of previously calculated[18] dependences on distance from the spacecraft of impact-excited radiances in three wavelength regions. These had been compiled for 0.01 g/s of water outgassing uniformly in angle around the spacecraft. As they refer to incident air at 75% higher density and 15% lower relative velocity than for *Discovery's* venting conditions, the plots are intended to be only semiquantitative representations of views normal to the ram, wake, and perpendicular-to-trajectory directions. The corresponding foreground radiances presented to sensors looking out from onboard are to a reasonable approximation one-half these look-in values extrapolated to X = 0, with the following principal caveats. 1) Numerical errors are introduced by the finite resolution of the grid near the "point" source of water vapor, which lies in the same cell as the spacecraft and the sensors themselves; 2) the calculated radiances viewing antiparallel to the initial stream direction are upper limits, as the transport model does not take into account blocking of the initial retrograde-to-stream gas flow by Orbiter's body; and 3) the radiances when the vapor source is within or even near instrument fields of view–obviously, poor experiment practice–are likely to be substantially underestimated because the densities are higher there than implicitly adopted in scaling the outgas results.

The brightness profile shapes are broadly similar for emission features other than these summed rotational lines and the two overlying principal short wavelength infrared bands, which with the cross-sections applied have about equal excitation probabilities[5,18]. A further caveat 4) is that the brightnesses near 6.3 μm looking out into the hemisphere into which the water is vented are about twice those predicted from collisional impact at 329 km altitude due to emission within about ~30 m from their evolution point by H_2O molecules that evaporate from the stream or droplets in the 010 state. As this last radiation tends to originate within the hyperfocal distance of optical sensors with very narrow fields of view, its degrading effect on their performance is somewhat ameliorated[25]. These adapted results and those in Fig. 7 indicate that the contaminating optical foreground from flash-evaporated water is reasonably isotropic (away from a region extending in both directions through the vented stream, which obviously presents computational difficulties), and lend themselves to comparison with the estimates in Table 2 of the spectrally-continuous radiances viewing into the limited solid angle occupied by the cloud of liquid/solidified water particles.

Figure 7 is a plot of look-in brightnesses in the (1,0) vibrational band of electronic ground-state hydroxyl, whose Q branch is at 2.80 μm and whose rotational width when produced by atom exchange is not known (¼ eV is a plausible estimate). The calculations refer to *Discovery's* venting and the other input parameters stated above, except that the populations of the first vibrational level of OH have been multiplied by two as a first approximation to taking into account cascading following the analogous population of higher levels. The essentially-spherical symmetry of the inner (higher) contours shows that this infrared foreground would be almost uniform in elevation and azimuth viewing from the spacecraft away from the above-noted zone in which the numerical method is unreliable, with a magnitude that we calculate to be 1×10^{-9} W/cm^2 sr. (This figure is in satisfactory agreement with the plot of SWIR radiances in Fig. 6, in which the H_2O stretch bands are also included but cascade of $OH^\dagger$ is neglected.) The asymmetry of the more distant contours about the trajectory direction is an artifact of limited numerical precision of the calculation. Their distinct "drag" toward the wake shows that after water dumps end at this altitude the 7¾ km/s-velocity spacecraft outruns the gaseous radiation source within $\lesssim$1 s; emission from the exhaust gases of Orbiter's thruster rocket engines shows a similar effect[30]. However water molecules that had adsorbed on surfaces could lead to longer-persisting optical foregrounds as they offgas at later times.

About equal collisionally-excited radiances are predicted in the sum of the two water bands near 2.7 μm and the 6.3 μm band, and also in the aforementioned arrays of pure-rotational lines[18]. An order of magnitude less total energy[26] would be emitted in each of the final three vibrational features listed above. In comparison under *Discovery*-like venting conditions optical sensors in the payload bay whose fields intercept the particulate trail proper at (typical) X = 20 m would encounter essentially spectrally-continuous contaminating daytime foregrounds of about 10^{-9} W/cm^2 sr between 2½ and 3½ μm–with which the almost completely surrounding, spectrally-structured radiance from the evolved vapor is comparable–, and 10^{-7} W/cm^2 sr between 8 and 13 μm–very much higher than in other pointing directions.

7. ACKNOWLEDGMENTS

Important contributions to the experiment and analysis program whose results are summarized in sections 2 and 3 of this paper were made by other USAF, NASA, AMOS, and contractor personnel, in particular G. Ashley, J. P. Bagian, J. Baird, A. Berk, J. F. Büchli, L. Dungan, J. B. Elgin, R. C. Garner, M. E. Gersh, Lt T. Hols, Maj E. Imker, D. J. Knecht, M. A. Maris, R. B. Sluder, N. H. Tran, C. A. Trowbridge, and L. Twist. R. C. Garner and P. J. McNicholl of PhotoMetrics provided valuable input on water-particle optics and rates of vapor evolution.

8. REFERENCES

1. C. P. Pike, D. J. Knecht, R. A. Viereck, E. Murad, I. L. Kofsky, M. A. Maris, N. H. Tran, G. Ashley, L. Twist, M. E. Gersh, J. B. Elgin, A. Berk, A. T. Stair, Jr., J. P. Bagian, and J. F. Büchli, "Release of liquid water from the space shuttle," *Geophys. Res. Lett.*, Vol. 17, No. 2, pp. 139-142, Feb. 1990.

2. R. A. Viereck, E. Murad, C. P. Pike, I. L. Kofsky, C. A. Trowbridge, D. L. A. Rall, A. Setayesh, A. Berk, and J. B. Elgin, "Photometric analysis of a space shuttle water venting," in Proceedings of the 4th Annual Workshop on Spacecraft Operations, Applications, and Research (SOAR '90), Albuquerque NM, June 1990, *NASA Conf. Pub.* 3103, pp. 676-680, 1991.

3. I. L. Kofsky, D. L. A. Rall, R. C. Garner, C. A. Trowbridge, E. Murad, C. P. Pike, D. J. Knecht, R. A. Viereck, A. Berk, M. E. Gersh, J. B. Elgin, A. T. Stair Jr., and A. Setayesh, "Photometric analysis of the venting of water from space shuttle," Paper 3.2, Proceedings of the European Space Agency Workshop on Space Environment Analysis, ESA WPP-23, 9-12 Oct. 1990.

4. I. L. Kofsky, D. L. A. Rall, M. A. Maris, N. H. Tran, E. Murad, C. P. Pike, D. J. Knecht, R. A. Viereck, A. T. Stair, Jr., and A. Setayesh, "Phenomenology of a water venting in low earth orbit," accepted for publication in *Acta Astronautica*, 1992.

5. J. B. Elgin, D. C. Cooke, M. F. Tautz, and E. Murad, "Modeling of atmospherically induced gas phase optical contamination from orbiting spacecraft," *J. Geophys. Res.*, Vol. 95, No. A8, pp. 12197-12208, Aug 1990.

6. E. P. Muntz and M. Orme, "Characteristics, control, and uses of liquid streams in space," *AIAA J.*, Vol. 25, No. 5, pp. 746-756, May 1987.

7. J. A. Gardner II, D. L. A. Rall, I. L. Kofsky, A. Setayesh, and E. Murad, "Liquid dispersal study: A proposed space shuttle liquid release experiment," Paper AIAA-92-0793, 30th Aerospace Sciences Meeting, Reno NV, 6-9 Jan. 1992.

8. B. P. Curry, R. J. Bryson, B. L. Seibner, and J. H. Jones, "[Selected] Results from an experiment [on] venting an H_2O jet into high vacuum," AEDC Technical Reports TR-84-28 and TR-85-3, Jan. and June 1985.

9. H. Fuchs and H. Legge, "Flow of a water jet into vacuum," *Acta Astronautica*, Vol. 6, No. 13, pp. 1213-1226, Dec. 1979.

10. T. T. Kassal, "Scattering properties of ice formed by release of H_2O in vacuum," *J. Spacecraft Rockets*, Vol. 11, No. 1, pp. 54-56, Jan. 1974.

11. P. A. Bernhardt, "A critical comparison of ionospheric depletion chemicals," *J. Geophys. Res.*, Vol. 92, No. A5, pp. 4617-4628, May 1987.

12. J. S. Pickett, N. D'Angelo, and W. S. Kurth, "Plasma density fluctuations observed during space shuttle Orbiter water releases," *J. Geophys. Res.*, Vol. 94, No. A9, pp. 12081-12086, Sep. 1989.

13. H. Patashnick and G. Rupprecht, "Sublimation of ice particles in space," Martin-Marietta Technical Report ED-2002-1654, Denver CO, Mar. 1973.

14. J. W. Duff and J. B. Elgin, "Fuel dumps as an optical obscurant," Proceedings of the 1986 Meeting of the IRIS Specialty Group on Targets, Backgrounds, and Discrimination, Vol. 1, pp. 137-146, July 1986.

15. R. D. Sharma and C. Buffalano, "Temperature and size histories of liquid H_2, O_2 and H_2O particles released in space," *J. Geophys. Res.*, Vol. 76, No. 1, pp. 232-237, Jan. 1973.

16. W. T. Rawlins and B. D. Green, "Spectral signatures of micron-sized particles in the shuttle optical environment," *Appl. Opt.*, Vol. 25, No. 15, pp. 3052-3060, Aug. 1987.

17. M. E. Fowler, L. J. Leger, M. E. Donahoo, and P. D. Maley, "Contamination of spacecraft by recontact of dumped liquids," Proceedings of the 3rd Annual Symposium on Space Operations, Automation, and Robotics (SOAR '89), *NASA Conf. Pub.* CL-3059, pp. 99-104, 1989.

18. M. M. Pervaiz, S. C. Richtsmeier, M. E. Gersh, and L. S. Bernstein, "Radiation estimates for collisionally excited outgassed molecules," in Proceedings of the Vehicle-Environment Interactions Conference (ed's. R. E. Erlandson and C. -I. Meng), Applied Physics Laboratory-Johns Hopkins University, 11-13 Mar. 1991.

19. M. R. Torr and D. G. Torr, "Gas phase collisional excitation of infrared emissions in the vicinity of the space shuttle," *Geophys. Res. Lett.*, Vol. 15, No. 1, pp. 95-98, Jan. 1988.

20. L. T. Melfi, J. E. Heuser, and F. J. Brock, "Direct simulation Monte Carlo technique for modeling of the environment in the vicinity of the space shuttle Orbiter," *SPIE* Proceedings, Vol. 287, Paper 10, 1981.

21. S. G. Warren, "Optical constants of ice from the ultraviolet to the microwave," *Appl. Opt.* Vol. 23, No. 8, pp. 1206-1225, April 1984.

22. G. R. Carruthers and J. S. Morrill, "Far ultraviolet cameras observations of airglow, auroras, and stellar occultations: quick look results," Paper SA21B-1, Proceedings of the AGU Fall Meeting, 9-13 Dec. 1991.

23. T. C. Degges and H. J. P. Smith, "A high altitude infrared radiance model," AFGL Technical Report TR-77-0271, 30 Nov. 1977.

24. D.E. Koch, G. G. Fazio, W. Hoffman, G. Melnick, G. Reike, J. Simpson, F. Witteborn, and E. Young, "Infrared observations of contaminants from shuttle flight 51-F," *Adv. Space Res.*, Vol. 7, No. 5, pp. 211-223, May 1987.

25. S. J. Young and R. R. Herm, "Model for radiation contamination by outgassing from space platforms," *J. Spacecraft Rockets*, Vol. 25, No. 6, pp. 413-420, Nov.-Dec. 1988.

26. R. E. Meyerott, G. R. Swenson, E. L. Schweitzer, and D. G. Koch, "Excitation of the low lying vibrational levels of H_2O by O ^3P as measured on Spacelab 2," in Proceedings of the Vehicle-Environment Interactions Conference (ed's. R. E. Erlandson and C. -I. Meng), Applied Physics Laboratory-Johns Hopkins University, 11-13 Mar. 1991.

27. J. Crovisier, "The water molecule in comets: fluorescence mechanisms and thermodynamics of the inner coma," *Astron. Astrophys.*, Vol. 130, pp. 361-372, 1974.

28. J. W. Duff, S. C. Richtsmeier, L. S. Bernstein, H. K. Burke, and M. Pietrzyk, "Analysis of HAVE SLED II flight test water outgassing," Proceedings of the 1992 Meeting of the IRIS Specialty Group on Targets, Backgrounds, and Discrimination, pp. 9-19, Mar. 1992.

29. M. Heninger, S. Fenistein, G. Mauclair, R. Marx, and E. Murad, "Review of the reaction of O^+ with H_2O and its bearing on composition measurements from the space shuttle," *Geophys. Res. Lett.*, Vol. 16, No. 2, pp. 139-141, Feb. 1989.

30. A. L. Broadfoot, E. Anderson, P. Sherard, D. J. Knecht, R. A. Viereck, C. P. Pike, E. Murad, J. E. Elgin, L. S. Bernstein, I. L. Kofsky, D. L. A. Rall, J. Blaha, and F. L. Culbertson, "Spectrographic observation at wavelengths near 630 nm of the interaction between the atmosphere and space shuttle exhaust," accepted for publication in *J. Geophys. Res.*, 1992.

Table 1. Summary of Numerical Results of the *Discovery* Water-Dumping Experiment*

Quantity	Magnitude	Comment
Fragmentation-particle radius	0.13 cm ±20% (mean), little decrease in 2½ km	"Average" figure derived from the constraint; about twice the radius of the venting orifice
Fragmentation-particle mass fraction, density	98% when formed (~88% in the AMOS views), 120 per meter	Follows from Fig. 5, and estimated from the onboard video photographs
Recondensation-particle radius	0.3 ±0.05 μm initially, decreases with X as in Fig. 4	Derived from the best-fit to radiances data; transitions to Rayleigh-scatter
Recondensation-particle mass fraction, density	0.022 ± 0.007 of the initially-vented water, 2½ × 10^{11} per m	Derived from constraint from irradiances at the image planes of cameras at long and short ranges
Longitudinal particle velocity	23 m/s +5, − 8 m/s (systematic error)	Measured from sequential video images; indistinguishable from the radially-relaxed stream
Transverse particle velocity	3–4 m/s nominal average	Little kinetic energy is imparted by fragmentation
Particle temperatures	Small 180K, in < 1 s Large 182K, in ~100 s	At equilibrium; refer to Fig. 4
Recondensation-particle cloud brightness 0.4–0.65 μm, at 48° and 33° aspect angle	2 x 10^{-6} W/cm² sr in a projection intercepting the symmetry axis at 1 km from the spacecraft	Calculated from the fractional water mass in and radius of these small droplets; see Fig. 2a

* 19.4 g/s of largely gas-free ~300K fuel cell product water vented at 329 km altitude in the daytime at low latitude through a 0.14-cm diameter 60°-conical nozzle.

Table 2. Optical Radiations from the Water Trail at Other than Visible Wavelengths

Water Component	Initial Fraction	Spatial Distribution	UV Radiance	SWIR Radiance	LWIR Radiance
Fragmentation Water/Ice Particles	0.84	As Fig. 2; X^{-2} uniformly in cone	Geometric sunlight scattering	Emissivity ≈ 1; weak scatter, weak thermal*	Negligible scatter, some thermal*
Recondensation Ice Particles	0.02	As Fig's. 1 and 2; X^{-2} in cone	Substantial near-Rayleigh scattering	Weak scatter, very weak thermal*	Very weak earth-shine scatter and thermal
Unrecondensed Vapor	0.14	See Fig's. 6 and 7	Negligible molecular scattering	Impact excitation and weak solar scatter ν_3-ν_1, plus OH vibrational	Impact excitation of ν_2 and rotational lines, weak earthshine

*Viewing perpendicular to the trail axis at 1 m, 10^{-8} } 3-5 μm 10^{-6} } 8-13 μm Watts/cm²sr(band)

at 1000 m, 10^{-12} } 3-5 μm 10^{-12} } 8-13 μm Watts/cm²sr(band)

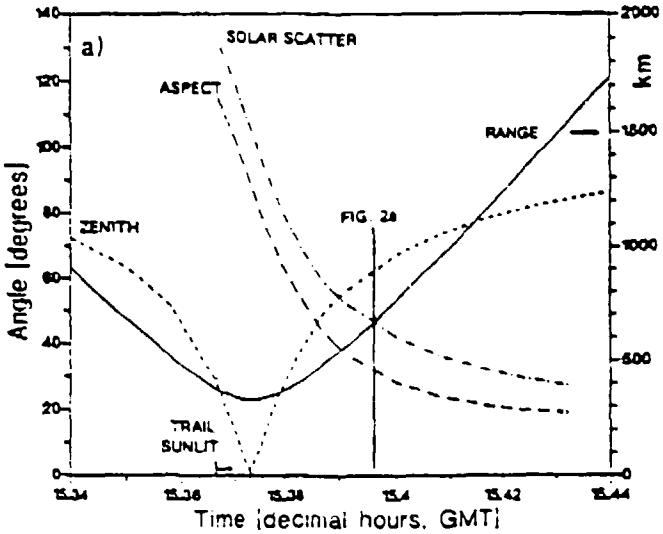

Fig. 1. AMOS viewing conditions for the *Discovery* water-venting experiment (16 Mar 1989).

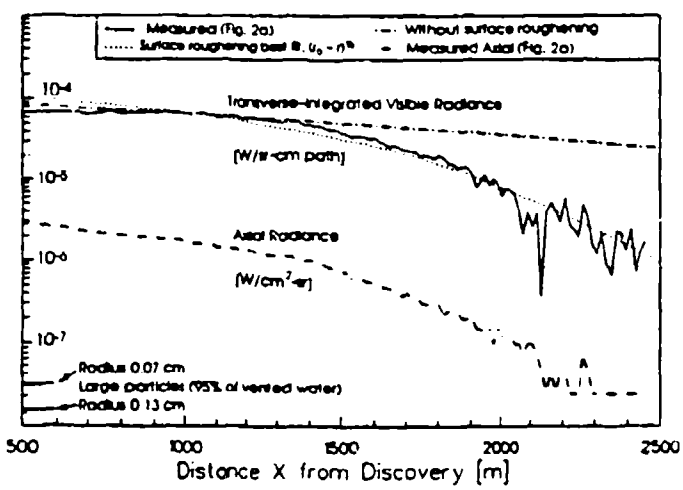

Fig. 3. Transverse and axial radiances extending downstream from spacecraft *Discovery* in Fig. 2a, with the normalized best fit to the time dependence of submicron particle radius as calculated in the text. (The slowly-sublimating large water-ice particles contribute little to the radiance signal at AMOS.)

Fig. 2. Views of the sunlit water trail from AMOS (0.3° horizontal angular field) and two video camera stations onboard *Discovery* (~34° field).

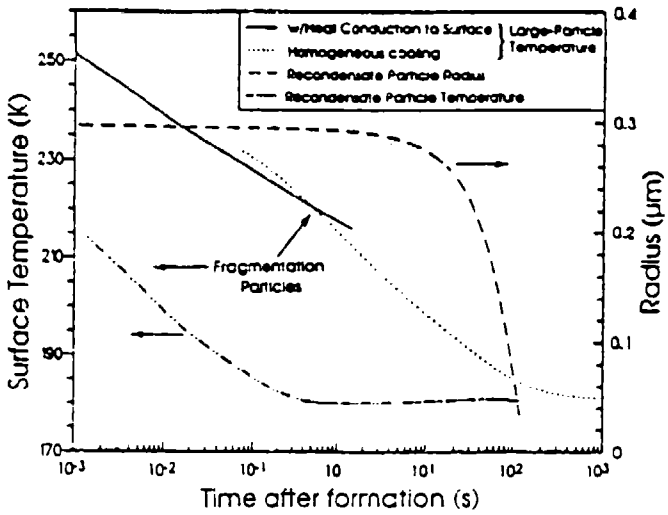

Fig. 4. Temperature and radius of the recondensation ice droplets derived from the AMOS video data and calculated temperature of the fragmentation particles.

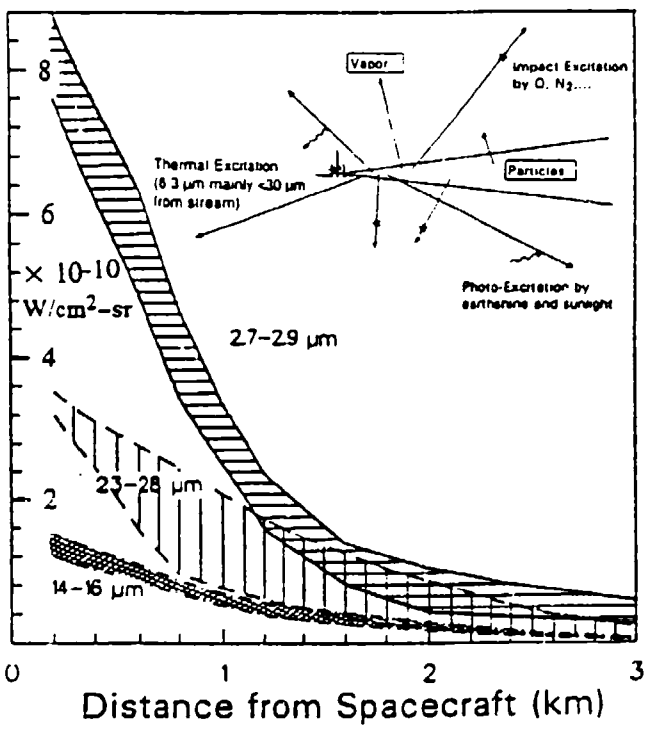

Fig. 6. "Look-in" radiances from the vapor collisionally excited in three infrared wavelength bands, scaled from direct simulation Monte Carlo calculations[18] for 6.6 km/s water outgassing at 300 km. The hatched areas indicate the variability among directly retrograde, posigrade, and perpendicular-to-orbital track view directions. The insert illustrates the three processes that lead to infrared emission from the evolved gas.

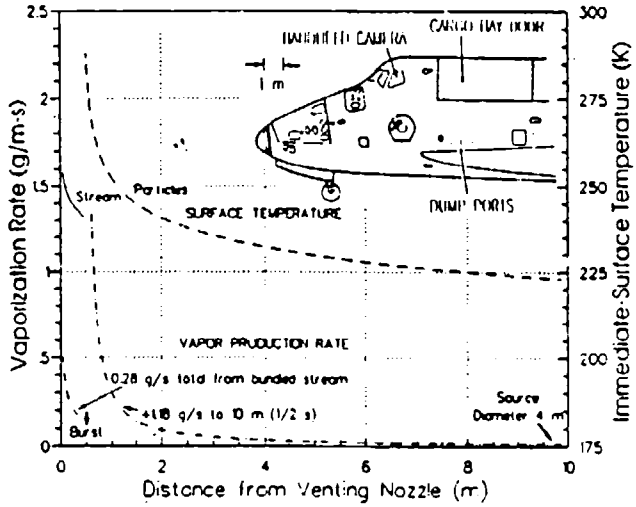

Fig. 5. Rate of evolution of water gas by evaporation/sublimation the coherent water stream and its fragmentation droplets. The insert shows the location of the venting orifice on Shuttle Orbiter's port side.

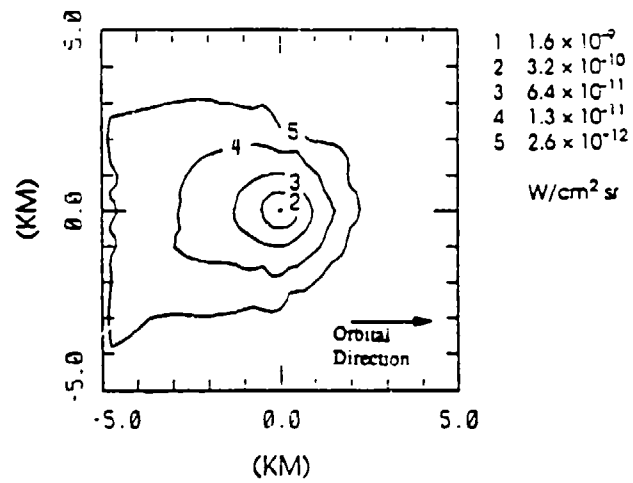

Fig. 7. "Look-in" radiances predicted by SOCRATES in the (1,0) vibrational band of OH for the venting conditions of *Discovery*. The corresponding foreground radiances looking out from the spacecraft (away from the stream direction) are nearly spherically uniform at 1 × 10^{-9} W/cm^2 sr. Total radiant intensity from the vapor reactions is 18 W/sr.